SIAM J. SCI. COMPUT.
Vol. 32, No. 5, pp. 3071–3091

PRECONDITIONED IMPLICIT SOLVERS FOR NONLINEAR PDEs IN MONUMENT CONSERVATION*

MATTEO SEMPLICE†

Abstract. Mathematical models for the description, in a quantitative way, of the damages induced on monuments by the action of specific pollutants are often systems of nonlinear, possibly degenerate, parabolic equations. Although some of the asymptotic properties of the solutions are known, one needs a numerical approximation scheme in order to have a quantitative forecast at any time of interest. In this paper an implicit numerical method is proposed, analyzed, and numerically tested for parabolic equations of porous media type and on a systems of two PDEs that models the sulfation of marble in monuments. Due to the nonlinearity inside the differential operator of the underlying mathematical model, the use of an iterative solver for a large system of nonlinear equations is required, and every step implies the solution of large, locally structured, linear systems. A special effort is devoted to the spectral analysis of the relevant matrices and to the design of appropriate iterative solvers, with special attention to preconditioned Krylov methods and to multigrid procedures. Numerical experiments for the validation of the analysis complement this contribution.

Key words. porous media, nonlinear parabolic equations, finite differences, multigrid preconditioning

AMS subject classifications. 65M55, 65M06, 76S05

DOI. 10.1137/100785417

1. Introduction.

The problem of monitoring, preserving, and, when needed, restoring monuments and works of art has become more and more relevant in recent years for the conservation of our cultural heritage, after the recognition of the negative effects of some pollutants on the monuments. Numerous studies made researchers and restorers increasingly aware that gaseous pollutants, atmospheric particulate matter, and some microorganisms can adversely affect the status of our monuments. In order to monitor the cultural heritage and to program restoration works, it is of paramount importance to be able to accurately assess the status of each monument. Along these lines, quantitative methods are emerging and making their way into the practice of preservation and restoration. These have the obvious advantages of allowing fair comparisons of the states of different monuments, and supporting the decision process on what to restore, clean, etc. and on the relative urgency of each case.

As an example, consider the *black crusts* that grow on marble surfaces as an effect of sulfation of the carbonate stone that is turned into gypsum when reacting with SO_2 in a moist environment. Since urban concentrations of SO_2 can nowadays be more than 100 times higher than the atmospheric basal values, this effect has become very important in recent decades. Sulfation can cause permanent damage to the monuments because gypsum crusts can be easily eroded by rain or (when located in protected areas) can become unaesthetically black with particulate matter from the atmosphere and eventually exfoliate [17, 11, 5].

A better scheduling of cleaning or deeper restoration can be devised if the thickness (and composition) of the crust can be forecasted in a quantitative way, providing a way to compute and thus predict the time evolution of the crust. The most common

*Received by the editors February 8, 2010; accepted for publication (in revised form) July 20, 2010; published electronically October 12, 2010.
http://www.siam.org/journals/sisc/32-5/78541.html
†Dipartimento di Fisica e Matematica, Università dell'Insubria - Sede di Como, Via Valleggio 11, 22100 Como, Italy (matteo.semplice@uninsubria.it).

quantitative evaluation of the sulfation phenomena that is used in practice consists of assuming that the thickness is directly proportional to the length of time of the exposure to the pollutants, with a proportionality coefficient obtained by fitting data from a large number of monuments [18]. Although this may give an average indication that is good enough for civil buildings, the uniqueness and cultural importance of a work of art calls for a more detailed analysis that can take into account the local environment to which the monument is exposed. Recently, a mathematical model of the sulfation of marble based on the chemical reactions involved was developed by Natalini and coworkers [2, 14] at IAC-CNR (Rome) and tested against experiments; see [12].

It is worthwhile to remark that the mathematical model is able to provide new information, which partly contradicts the most common quantitative evaluation methods based on data fitting. In particular (see [15]), the asymptotic study of the equations in a one-dimensional setting reveals that for large times the thickness of the gypsum crust does not grow proportionally to the elapsed time as in the Lipfert formula, but proportionally to its square root: the speed of growth of the crust is significantly reduced as time goes on. Clearly this means that a complete removal of the crust will speed up the damage and it calls for study of optimal strategies for periodic partial crust removal.

However, the asymptotic analysis does not give enough information on what happens for short times and, moreover, the study is not yet available for complex geometries. For example, on a corner stone, SO_2 penetrates the marble from two sides: how does the crust grow? Does it get rounded? By how much? And, more importantly, what about the fine features of decorations or statues? In some cases sulfation has caused an almost complete loss of detail: can the model predict the thickness of the crust there and allow the scheduling of an optimal conservation strategy? In order to answer the previous questions, one needs a numerical method to solve the equations of the model developed in [2]. This is a system of two equations, one of which is nonlinear of parabolic type.

This paper generalizes and applies the novel numerical techniques studied in [9] to integrate for long times nonlinear, possibly degenerate, parabolic equations such as those appearing in the model in [2]. The techniques developed here, however, have applications that go beyond the aforementioned model. For example, in the area of *planned conservation*, the techniques could be adapted to numerically investigate the more complete sulfation model described in [1] and the consolidation model presented in [7].

This paper considers two fully implicit discretizations in time, thus solving a nonlinear system at each timestep. In order to fix ideas, consider the parabolic equation

$$\frac{\partial u}{\partial t} = \nabla \cdot (D(u)\nabla u)\,, \tag{1.1}$$

where $D(u)$ is a nonnegative differentiable function, and denote with $\mathcal{L}_D(u)$ the elliptic operator on the right-hand side.

In the literature, degenerate parabolic equations have been discretized mainly using explicit or semi-implicit methods, thus avoiding solving the nonlinear equations. A remarkable class of methods arise directly from the so-called nonlinear Chernoff formula [4] for time advancement, coupling it with a spatial discretization: for finite differences this was started in [3], and for finite elements in [19]. The schemes in this class share a timestep restriction of the form $\Delta t = O(h^2)$ for stability, but, especially in the finite element setting, there is a mature theory that also includes

error estimators and h-adaptivity. For example, the numerical scheme analyzed in [2] for integrating the sulfation model belongs to the class of semi-implicit methods. More recently, another class related to the relaxation approximation emerged: such numerical procedures exploit high order nonoscillatory methods typical of the discretization of conservation laws, and their convergence can be proved making use of semigroup arguments similar to those relevant for proving the Chernoff formula [6]. Finally, we wish to point out the paper [10], where the authors derive conservative schemes for degenerate convection diffusion equations with the elliptic operator in the form $\partial^2_{xx}(K(u))$, which is obviously equivalent to (1.1) in one space dimension, setting $K(u) = \int_0^u D(\xi)\mathrm{d}\xi$.

In this paper, however, we chose to use form (1.1) since most models arise naturally in this form, where $D(u)$ has the direct physical interpretation of diffusion coefficient. Especially in two dimensions, it is not trivial to turn form (1.1) into that required by the scheme described in [10], and if (in one space dimension) one does not have a closed form expression for $K(u)$ and thus approximates the integral with the midpoint rule, Evje and Karlsen's discretization of the elliptic operator falls back to the one used in this paper.

Thus, denoting with U the numerical solution of (1.1), and considering a time discretization so that $\Delta t = t^n - t^{n-1}$, in this paper we employ the (first order accurate) implicit Euler scheme

$$U(t^n, x) - \Delta t \mathcal{L}_D(U(t^n, x)) = U(t^{n-1}, x) \tag{1.2}$$

and the (second order accurate) Crank–Nicholson scheme

$$U(t^n, x) - \frac{\Delta t}{2}\mathcal{L}_D(U(t^n, x)) = U(t^{n-1}, x) + \frac{\Delta t}{2}\mathcal{L}_D(U(t^{n-1}, x)). \tag{1.3}$$

(Note that (1.2) is also known as the Crandall–Liggett formula, after [8].)

The computation of $U(t^n, x)$ with (1.2) or (1.3) requires us to solve a nonlinear equation whose form is determined by the elliptic operator and the nonlinear function $D(u)$, but the convergence is guaranteed without restrictions on the timestep Δt. Due to the nonlinear nature of the underlying mathematical model, the use of a fixed point scheme is required, and the choice of the faster Newton-like methods implies the solution at every step of large, locally structured (in the sense of Tilli; see [24, 23]) linear systems. A special effort was devoted in [9] to the spectral analysis of the matrices arising from (1.2) for scalar equations and to the design of appropriate iterative or multi-iterative solvers (see [22]), with special attention to preconditioned Krylov methods and to multigrid procedures (see [13, 21, 16, 25] and the references therein for a general treatment of iterative solvers). This paper shows that those methods can be extended to the case of (1.3) and to systems and can perform numerical tests on the model of [2].

The paper is organized as follows. In section 2 the results of [9] on scalar equations are recalled and extended to the case of a scheme which is second order in time, including numerical tests. In section 3 the sulfation model is described, and section 4 concerns the corresponding implicit numerical scheme and the preconditioners for the linear systems. Next, we present numerical tests on the model in one spatial dimension in section 5 and in two spatial dimensions in section 6. Finally, section 7 contains some possible developments of this work.

2. Scalar equations. In this section, the case of a single equation of the porous media type is considered, namely (1.1), where $D(u)$ is a nonnegative differentiable

function. The parabolic equation is of degenerate type whenever $D(u)$ vanishes for some values of u. The convergence analysis of the numerical methods requires that $D(u)$ be at least continuously differentiable, while the existence of solutions is guaranteed under the milder assumption of continuity [26]. Most applications of the porous media equation involve $D(u) = u^m$ for some positive m.

For this particular choice, the following self-similar exact solutions have been computed by Barenblatt and Pattle (see [26]):

$$u(t,\mathbf{x}) = t^{-\alpha}\left[1 - k\left(\frac{|\mathbf{x}|}{t^{\alpha/d}}\right)^2\right]_+^{\frac{1}{m-1}} \qquad \text{for } t > 0, \mathbf{x} \in \mathbb{R}^d, \tag{2.1}$$

where $|\mathbf{x}| = \sqrt{\sum_1^d x_i^2}$ and $\alpha = \frac{d}{d(m-1)+2}$, $k = \alpha\frac{m-1}{2md}$. These solutions are singular for $t = 0$, but for $t > 0$ represent important reference cases both for the analysis of the solutions of (1.1) and for numerical tests.

Here, results of [9] on scalar equations are recalled and extended to the case of a scheme which is second order in time. They will be used in section 3, which deals with a system of two equations, since the linear systems arising there include, as a subsystem, those considered in this section.

2.1. Numerical scheme. In order to obtain a numerical scheme for approximating the solutions of (1.1), first the time variable is discretized with the Crank–Nicholson formula (1.3), generalizing the simpler case of implicit Euler that was considered in [9]. It is worth pointing out that searching for high order schemes for (1.1) would seem useless at first, since the exact solution of the equation is in general continuous but not differentiable, so any scheme would converge, in theory, with order 1. However, in practice, the exact solution is often piecewise regular, allowing a higher order scheme to converge faster than first order and in any case to achieve better errors than (1.2) at a given spatial resolution, even if the theoretical order of convergence is not reached.

The discretization is then completed by considering the points $x_k = a + kh$ in the spatial domain $[a, b]$, where $h = (b - a)/(N + 1)$ and $k = 0, \dots, N + 1$, and approximating the one-dimensional nonlinear elliptic operator with the usual 3-point finite difference formula, i.e.,

$$\begin{aligned}\frac{\partial}{\partial x}\left(D(u)\tfrac{\partial u}{\partial x}\right)\Big|_j &= \frac{D(u)_{j+1/2}\ \frac{\partial u}{\partial x}\big|_{j+1/2} - D(u)_{j-1/2}\ \frac{\partial u}{\partial x}\big|_{j-1/2}}{h} + o(1)\\ &= \frac{(D(u_{j+1}) + D(u_j))(u_{j+1} - u_j) - (D(u_j) + D(u_{j-1}))(u_j - u_{j-1})}{2h^2} + o(1).\end{aligned} \tag{2.2}$$

In order to write down the numerical scheme compactly, collect in a vector $\mathbf{u}^n$ all the unknown values $u_j^n = u^n(x_j)$. For example, when Dirichlet boundary conditions are considered, since u_0 and u_{N+1} are known, $\mathbf{u}^n$ has N elements, namely $u_1^n, \dots, u_N^n$.

In the following, the notation $\text{tridiag}_k^N[\beta_k, \alpha_k, \gamma_k]$ is for a square tridiagonal matrix of order N with entries β_k on the kth row of the lower diagonal, $k = 2, \dots, N$, α_k on the main diagonal, $k = 1, \dots, N$, and γ_k on the upper diagonal, $k = 1, \dots, N - 1$. Moreover, $\text{diag}^N[\alpha_k]$ indicates an order N square diagonal matrix with α_k on the kth row. Recalling that (1.3) is a second order approximation, one has

$$\mathbf{u}^n - \mathbf{u}^{n-1} = \frac{1}{2}\frac{\Delta t}{h^2}L_{D(\mathbf{u}^n)}\mathbf{u}^n + \frac{1}{2}\frac{\Delta t}{h^2}L_{D(\mathbf{u}^{n-1})}\mathbf{u}^{n-1} + o(\Delta t^2 + h^2), \tag{2.3}$$

where

$$L_{D(\mathbf{u})} = \text{tridiag}_k^N[D_{k-1/2}, -D_{k-1/2} - D_{k+1/2}, D_{k+1/2}] \tag{2.4}$$

and

$$D_{j+1/2} = \frac{D(u_{j+1}) + D(u_j)}{2},\ j = 0, \ldots, N.$$

In two dimensions, on the finite grid composed by the $(N+2) \times (N+2)$ points $\mathbf{x}_{i,j} = \mathbf{a} + ih\mathbf{e}_1 + jh\mathbf{e}_2$, where $\mathbf{a}$ is the lower left corner of the domain, h the discretization parameter, $\mathbf{e}_l$ $(l = 1, 2)$ the unit vectors along the coordinate axis, and $i, j \in \mathbb{N}$, the matrix $L_{D(\mathbf{u})}$ approximating $\nabla \cdot (D(u^n)\nabla u^n)$ is pentadiagonal. When considering Dirichlet boundary conditions, adopting the usual lexicographic ordering of the unknowns $u_{i,j}^n$, $L_{D(\mathbf{u})}$ is a $N^2 \times N^2$ square matrix, and nonzero entries can be found only on the main diagonal, the first, and the Nth upper and lower diagonal.

Finally, note that, as argued in [23], the asymptotic spectral properties of the matrices arising from this discretization (L_D in our case) to a large extent do not depend on the choice of the finite difference formula, but really depend on the locally Toeplitz structure that in turn arises from an operator appearing in the PDE. Thus it should be possible to generalize most of the results of the following sections on linear solvers and preconditioning to other spatial discretizations techniques, including finite element methods.

2.2. Newton method. In order to advance the numerical solution from $\mathbf{u^{n-1}}$ to $\mathbf{u^n}$, the nonlinear system of equations (2.3) must be solved at each timestep. This is achieved by iterating with Newton's method for the function

$$F(\mathbf{u}) = \mathbf{u} - \frac{1}{2}\frac{\Delta t}{h^2} L_{D(\mathbf{u})}\mathbf{u} - \frac{1}{2}\frac{\Delta t}{h^2} L_{D(\mathbf{u}^{n-1})}\mathbf{u}^{n-1} - \mathbf{u}^{n-1}. \tag{2.5}$$

The Jacobian of F is

$$F'(\mathbf{u}) = X_N(\mathbf{u}) + Y_N(\mathbf{u}), \tag{2.6}$$

$$X_N(\mathbf{u}) = I_N - \frac{1}{2}\frac{\Delta t}{h^2} L_{D(\mathbf{u})}, \tag{2.7}$$

$$Y_N(\mathbf{u}) = -\frac{1}{2}\frac{\Delta t}{h^2} T_N(\mathbf{u})\,\text{diag}_k^N(D_k'), \tag{2.8}$$

$$T_N(\mathbf{u}) = \text{tridiag}_k^N[u_{k-1} - u_k, u_{k-1} - 2u_k + u_{k+1}, u_{k+1} - u_k], \tag{2.9}$$

where T_N is the same matrix of the implicit Euler case analyzed in [9]. (In two space dimensions, T_N would be pentadiagonal.)

The first order scheme based on implicit Euler gives rise to

$$\widetilde{F}(\mathbf{u}) = \mathbf{u} - \frac{\Delta t}{h^2} L_{D(\mathbf{u})}\mathbf{u} - \mathbf{u}^{n-1}. \tag{2.10}$$

This is the case studied in [9]. Since the Jacobian matrix of $\widetilde{F}$ differs from F' only for the $\frac{1}{2}$ factors in X_N and Y_N, most of the results proved in [9] can be adapted to the present setting. Thus the proofs in this section will only be sketched.

Our main result is that the Newton method defined by F, initialized with $\mathbf{u}^{n,0} = \mathbf{u}^{n-1}$, is convergent under a linear restriction on the timestep.

THEOREM 2.1. *The Newton method for $\widetilde{F}(\mathbf{u})$ defined in* (2.5) *for computing $\mathbf{u}^n$ is convergent when initialized with $\mathbf{u}^{n,0} = \mathbf{u}^{n-1}$ (i.e., the solution at the previous timestep) and for $\Delta t \le Ch$, for a positive constant C independent of h.*

Proof. The proof of the same statement for F, based on the Kantorovich theorem (see, e.g., [20]), given in [9], can be adapted easily to the present case.

The key point is again to show that there exists C_∞, C_1 independent of h such that

$$\left\|F'(\mathbf{u})^{-1}\right\|_\infty \le C_1, \tag{2.11}$$

provided that $\Delta t \le C_\infty h$. For this, note that $F'(\mathbf{u})$ differs from $\widetilde{F}'(\mathbf{u})$ for $\widetilde{F}$ defined in (2.10) only by factors $\frac{1}{2}$ appearing before any $D_{k+1/2}$ term. Since these terms are discarded in the estimates in the proof, the proof of Proposition 2.1 of [9] can be generalized to the present setting. ∎

Remark 2.2. Setting the initial guess with the average between $\mathbf{u}^{n-1}$ and the value given by an explicit Euler step such as

$$\mathbf{u}^{n,0} = \mathbf{u}^{n-1} + \frac{1}{2}\frac{\Delta t}{h^2} L_{D(\mathbf{u}^{n-1})}\mathbf{u}^{n-1}$$

does not change the convergence ratio, but in practice one needs fewer iterations to reach a given tolerance.

2.3. Iterative methods for the linear system. Of course the $(s+1)$th Newton iterate is computed by first solving the linear system

$$F'(\mathbf{u}^{n,(s)})\mathbf{v}^{(s)} = F(\mathbf{u}^{n,(s)})$$

for $\mathbf{v}^{(s)}$ and then setting

$$\mathbf{u}^{n,(s+1)} = \mathbf{u}^{n,(s)} + \mathbf{v}^{(s)}.$$

The matrix $A_N = F'(\mathbf{u}^{n,(s)})$ is a square tridiagonal (respectively, pentadiagonal) $N \times N$ (respectively, $N^2 \times N^2$) matrix when the domain is one- (respectively, two-) dimensional. Its spectral properties are crucial in choosing an appropriate solver for the linear system. Given the large dimension of the system, an iterative method with an optimal preconditioner would allow us to compute $\mathbf{v}^{(s)}$ in a number of iterations, which is independent of the system size.

Moreover, A_N differs from $\widetilde{F}'$ only by the factors $\frac{1}{2}$ that were missing in the matrices studied in [9]. It can thus be shown that, also in the present setting, A_N is not symmetric, but it is dominated by its symmetric part $(A_N + A_N^{\mathsf{T}})/2$, which is in turn essentially a weighted Laplacian. Rather detailed information on the spectrum of A can be gained via the theory of locally Toeplitz sequences in [24]. In particular, when Δt is chosen proportional to h, the sequence of $N \times N$ matrices $\{hA_N\}$ obtained for an increasing number of grid points is locally Toeplitz (in the sense of [24]) with respect to the pair of functions $(D(u(x)), 2 - 2\cos(s))$ defined on $[a, b] \times [0, 2\pi]$. Hence (see [9]) the GMRES method, which is picked as the main iterative solver due to the asymmetry of A_N, is expected to converge in $O(\sqrt{N})$ iterations.

In order to study a preconditioning strategy, first observe that the sequence $\{X_N\}$ defined by (2.7) is also locally Toeplitz with respect to the same generating functions. Next recall that any locally Toeplitz sequence is also generalized locally Toeplitz, a class which is closed under inversion, defined in [23]. Hence both sequences are also

generalized locally Toeplitz sequences, and $\{X_N^{-1}A_N\}$ is generalized locally Toeplitz with generating function 1, and thus the singular values are weakly clustered at the point 1. This is enough to guarantee the superlinear convergence of the preconditioned GMRES methods, but in [9] it is also shown that the clustering is strong, proving that X_N is an optimal preconditioner for solving a linear system with matrix $\{A_N\}$ with GMRES; i.e., a given error reduction is reached within a number of iterations which is independent of the problem size N.

Unfortunately there is not a fast direct solver for X_N, but a multigrid method (MGM) with a Galerkin approach can be successfully applied. The MGM [25] consists of constructing a solution of a linear system by composing the action of simple iterative schemes (like Jacobi or Gauss–Seidel) that are run on the original system and on smaller systems derived from the first one and called *coarse grid approximations*.

More precisely, in order to solve a linear system $X\mathbf{u} = \mathbf{b}$ in $\mathbb{R}^m$, one considers a finite sequence of integers $m_0 = m > m_1 > m_2 > \cdots > m_\ell > 0$ and full-rank matrices $P_{(i+1)}^{(i)} \in \mathbb{R}^{m_{i+1}\times m_i}$ (called *projections*), and defines the V-cycle method as

$$\mathbf{u^{k+1}} = MGM(0, \mathbf{u}^k, \mathbf{b}),$$

with MGM defined recursively as follows:

$$\mathbf{u}_i^{(\mathrm{out})} := MGM(i, \mathbf{u}_i^{(\mathrm{in})}, \mathbf{b}_i)$$

If $(i = \ell)$, then Solve$(A_\ell \mathbf{u}_\ell^{(\mathrm{out})} = \mathbf{b}_\ell)$

Else

1 $\widetilde{\mathbf{u}}_i := S_i^\nu\big(\mathbf{u}_i^{(\mathrm{in})}\big)$,

2 $\mathbf{r}_i := A_i\widetilde{\mathbf{u}}_i - \mathbf{b}_i$,

3 $\mathbf{b}_{i+1} := P_{(i+1)}^{(i)}\mathbf{r}_i$,

4 $A_{(i+1)} := P_{(i+1)}^{(i)} A_{(i)} (P_{(i+1)}^{(i)})^{\mathsf{T}}$,

5 $\mathbf{y}_{i+1} := MGM(i+1, \mathbf{0}_{n_{i+1}}, \mathbf{b}_{i+1})$,

6 $\mathbf{u}_i^{(\mathrm{out})} := \widetilde{\mathbf{u}}_i - (P_{i+1}^i)^{\mathsf{T}}\mathbf{y}_{i+1}$

Step 1 performs some (ν) iterations of an iterative method (called a *presmoother*) for n_i-dimensional linear systems (denoted generically as $\mathcal{S}_i$), chosen for its error dampening properties, which is often taken in the Jacobi or the Gauss–Seidel family. Then, step 2 calculates the residual of the proposed solution and steps 3–6 define the *recursive coarse grid correction*—by projection (step 3) of the residual, subgrid correction (steps 4, 5), and interpolation (step 6). Note that only the smallest system (of level ℓ) is solved exactly, while all the others are recursively managed by reduction to low-level systems and smoothing. For more details and generalizations, see, e.g., [25].

For differential problems, it is natural to construct the coarse grid approximations with the Galerkin approach, i.e., by considering a sequence of coarser and coarser grids with interpolation operators $P_{(l)}^{(l+1)}$ reconstructing values of the unknown function on the grid of level l from the smaller set values on the coarser grid of level $l+1$. In this paper it is sufficient to consider linear (bilinear in two dimensions) interpolation operators. This is known to give rise to an optimal solver for a weighted Laplacian. Moreover, in [9] it is also observed that it is not necessary to bring the MGM to convergence, but applying a single V-cycle to the GMRES residual is enough to optimally precondition the GMRES method.

Moreover, since Y_N is (spectrally) negligible with respect to X_N, the MGM V-cycle can be applied using the whole Jacobian matrix $F' = X_N + Y_N$ instead of X_N.

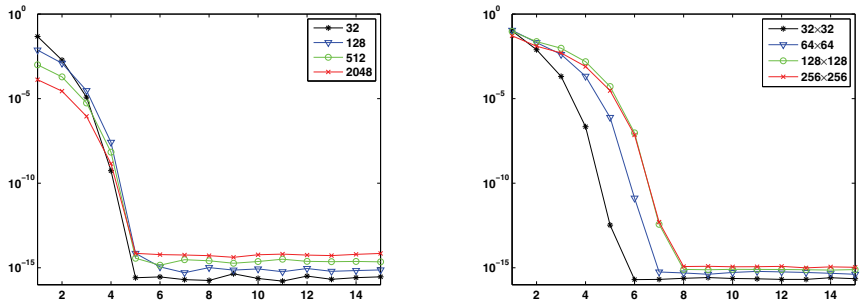

(a) (b)

FIG. 1. *Crank–Nicholson scheme: Newton convergence history in one* (a) *and two* (b) *spatial dimensions.*

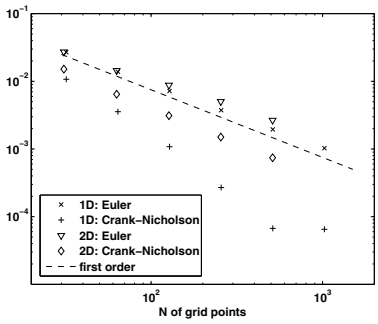

FIG. 2. *Error of the numerical scheme in one and two dimensions, compared with implicit Euler.*

This leads to a slight reduction of the number of GMRES iterations. The results reported in the next section refer to this preconditioning strategy.

2.4. Numerical tests. This section collects some numerical tests supporting the results previously described. For N ranging from 32 to 1024, equation (1.1) with the Barenblatt initial data (2.1) for $m = 2$ is integrated numerically from $t = 1$ to $t = 1 + 20/32$ in one and two spatial dimensions, recording the number of Newton iterations, GMRES iterations, and the error against the exact solution. Results for higher values of m are similar.

Figure 1 plots the quantity $\|\mathbf{u}^{1,s} - \mathbf{u}^{1,s-1}\|$ during the Newton iterations $s = 1, 2, \ldots, 30$ for computing the first timestep. Different symbols and line colors correspond to different mesh sizes on the interval (panel (a)) and on a square domain (panel (b)). It is clear that the very good tolerance 10^{-6} is reached within a reasonable number of iterations: four in one spatial dimension and six in $\mathbb{R}^2$. This good convergence history is to a large extent not dependent on the chosen value for m (see also [9]).

Using the Crank–Nicholson scheme, a reduction of the error with respect to the first order Euler scheme is observed (see Figure 2), even if the scheme does not converge with the expected order 2. This is due to the presence of singularities in the exact solution. The least square fit of the errors obtained in one dimension with the Crank–Nicholson scheme and represented with plus signs in the figure gives us that

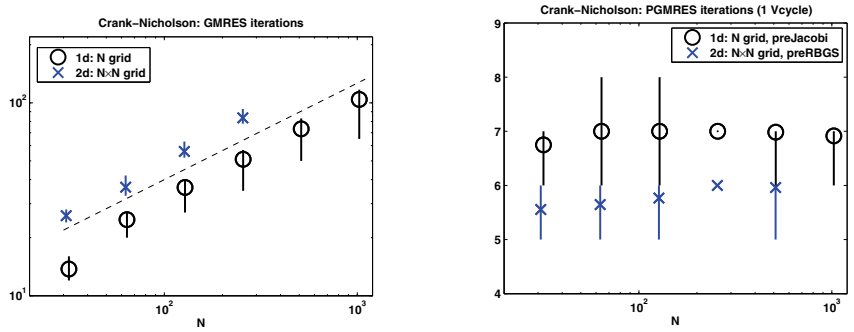

FIG. 3. *Crank–Nicholson scheme: GMRES iterations inside the Newton steps.* (a) *No preconditioning (the dashed line is the $N^{1/2}$ slope).* (b) *One V-cycle as preconditioner.*

the error decays proportionally to $N^{-1.5}$. In two dimensions the rate of convergence is closer to 1, but the errors are nevertheless lower than those obtained with the implicit Euler scheme.

Finally, Figure 3 shows the plot of the number of iterations of the methods for the linear system. For each value of N, the average number of GMRES iterations performed by the algorithm is indicated by the symbols, while the vertical lines span from the minimum to the maximum value recorded during the integration. Figure 3(a) compares the number of unpreconditioned GMRES iterations on different one- and two-dimensional grids with the $\sqrt{N}$ slope. Note that for the largest values of N, the two-dimensional experiments were not possible due to memory limitations on a PC with 8GB of RAM. The MGM used here as preconditioner had one damped Jacobi iteration as a presmoother in the V-cycle for the one-dimensional experiments, while in the two-dimensional tests the more efficient red-black Gauss–Seidel has been employed. Figure 3(b) shows that applying one MGM V-cycle is optimal (constancy of iterations number for different N), robust (small variance in iterations number), and memory efficient (small number of iterations require small amount of storage memory in GMRES without the need for the restarted procedure).

3. Marble sulfation. This section is about the numerical simulations of marble sulfation using the model introduced in [2]. The main features of the model are described only briefly; refer the reader to the original paper for the details and a more comprehensive study of the properties of the solutions. In [2], the authors consider the (simplified) chemical reaction

$$\mathrm{CaCO_3} + \mathrm{SO_2} + \frac{1}{2}\mathrm{O_2} + 2\mathrm{H_2O} \longrightarrow \mathrm{CaSO_4 \cdot 2H_2O} + \mathrm{CO_2}$$

to account for the transformation of $\mathrm{CaCO_3}$ of the marble stone into $\mathrm{CaSO_4 \cdot 2H_2O}$ (gypsum), which is triggered in a moist atmosphere by the availability of $\mathrm{SO_2}$ at the marble surface and inside the pores of the stone. The two main variables of the model are $c(t, x)$, denoting the local concentration of calcium carbonate, and $s(t, x)$, the local concentration of $\mathrm{SO_2}$. As the reaction proceeds, the calcium carbonate concentration is reduced from the initial value c_0, as $\mathrm{CaCO_3}$ is progressively replaced by gypsum. Denoting φ_0 and φ_g the porosity of the pristine marble and of the gypsum, the model assumes that the porosity of the intermediate state is well approximated by linear

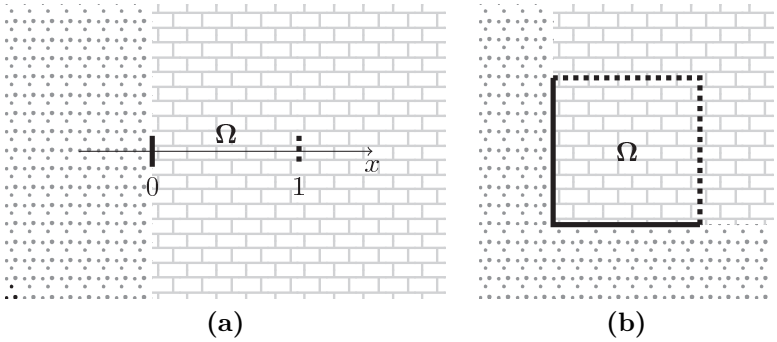

FIG. 4. *Sample domains* Ω *for problem* (3.1) *are shown for the one-dimensional setting* (a) *and the two-dimensional setting* (b). *The "brick pattern" area represents the marble stone, while the dotted area is air. The boundary is drawn with a solid line where Dirichlet boundary conditions are applied and with a dotted line where free-flow boundary conditions are imposed.*

interpolation

$$\varphi(c) = \varphi_g + (\varphi_0 - \varphi_g)\frac{c}{c_0} = \alpha c + \beta.$$

The constants α and β depend on the porosity of the material involved. The model considered in [2] is described by the following system of PDEs:

$$\begin{cases} \dfrac{\partial \varphi(c)s}{\partial t} = -\frac{a}{m_c}\varphi(c)sc + d\nabla\cdot(\varphi(c)\nabla s)\,, \\ \dfrac{\partial c}{\partial t} \qquad\quad = -\frac{a}{m_s}\varphi(c)sc. \end{cases} \tag{3.1}$$

The spatial domain $x \in \Omega$ in which (3.1) is set represents a piece of marble stone for which at least a portion of the boundary $\partial\Omega$ is in contact with the polluted atmosphere. In particular, $\partial\Omega$ is in general split into two parts: one represents the outer surface of the marble sample, in contact with the air, and the complementary part separates the portion of the marble object of the simulation and the rest of the monument.

Examples of such one- and two-dimensional such domains are shown in Figure 4. In order to study the formation of a gypsum crust on a flat area of a monument, it is sufficient to take a one-dimensional domain such as that shown in the panel (a). In order to study a corner-like feature of a work of art, such as the edge of a monument or a long decoration in relief, one would employ a two-dimensional domain as shown in panel (b). Obviously, more complex shapes need three-dimensional domains faithfully representing the volume occupied by the marble.

Boundary conditions are set by imposing the value of s on the outer boundary and free-flow conditions for s on the inner boundary. In particular, as an example of a one-dimensional setting, take $x \in \Omega = [0,1]$, where $x = 0$ corresponds to the outer boundary of the marble stone (in contact with the polluted air), and $x = 1$ to the inner boundary. The boundary conditions are illustrated in Figure 4: they are of Dirichlet type (imposing $s(0,t)$ on the outer boundary) and of free-flow type (imposing $\frac{\partial s}{\partial x}(1,t) = 0$ on the inner boundary).

The parameters m_s and m_c are fixed by the physical properties of the species involved in the reaction and ensure that the mass balance is fulfilled. On the other

hand, a represents the reaction rate, and it depends (among other things) on the moisture of the air and on the temperature. The authors of [2] describe its central role in the analysis of the solutions of the model equations. In particular, if $u(t,x)$ is a solution of (3.1) for a given value of a, then $\tilde{u}(t,x) = u(t/a^2, x/a)$ is a solution of (3.1) for $a = 1$. This observation on the one hand plays a fundamental role in establishing the long-time asymptotics of the solution, and would allow us to perform the simulations with $a = 1$ and then rescale the numerical solutions appropriately to take the reaction rate into account. However, because of the role of a as the fundamental physical parameter of the model, the form (3.1) of the equations was employed for the numerical simulations. Moreover, this is beneficial in view of the more complete model, including a nonconstant a, which has been described in [1].

In particular, as in [2], the values $\alpha = 0.01$, $\beta = 0.1$, $d = 1$, $m_s = 64.06$, $m_c = 100.09$ are used throughout, while a varies from 1 to 10^5.

4. Discretization of the sulfation model. The general setup for the scheme is the same as in the scalar case: first discretize the time variable using (1.3) and then discretize the spatial domain and the elliptic differential operator with finite differences, write the time-advancement problem as an implicit equation, and set up a Newton scheme to solve it. This procedure is convenient if the Newton scheme converges in a reasonable number of iterations and one can devise an optimal preconditioner for the linear system that has to be solved at each Newton step.

For the space discretization, denote $x_\xi = 0 + \xi h \in \Omega$. Approximating the elliptic operator along the same lines as in (2.2), consider the second order finite difference formula

$$\partial_x(\varphi(c)\partial_x s)|_{x_j} = \frac{\varphi(c(x_{j+1/2}))(s(x_{j+1}) - s(x_j))}{h^2} - \frac{\varphi(c(x_{j-1/2}))(s(x_j) - s(x_{j-1}))}{h^2}. \tag{4.1}$$

This in turn suggests employing two staggered grids in the domain Ω: the set of points x_j ($j \in \mathbb{N}$) carrying the unknowns s_j^n for $s(t^n, x_j)$ and the set of points $x_{j+1/2}$ ($j \in \mathbb{N}$) with the unknowns $c_{j+1/2}^n$ for $c(t^n, x_{j+1/2})$. The notation $\varphi_{j+1/2}^n = \varphi(c_{j+1/2}^n)$ will also be used. For ease of reference, the two grids are also called "integer grid" and "half-integer grid."

Here the formulas for the Crank–Nicholson time discretization (1.3) are considered, while the case of the Crandall–Liggett (implicit Euler) scheme (1.2) can be similarly dealt with. Thus consider the scheme that computes s_j^n and $c_{j+1/2}^n$ solving the nonlinear system of equations

$$\begin{cases} 0 = \mathbf{F}^{(s)}(\mathbf{s}^n, \mathbf{c}^n) = \Phi^n \mathbf{s}^n + \dfrac{\Delta t}{2}\dfrac{a}{m_c} C^n \mathbf{s}^n + \dfrac{\Delta t}{2} dL_{\varphi^n}\mathbf{s}^n \\ \qquad\qquad - \Phi^{n-1}\mathbf{s}^{n-1} + \dfrac{\Delta t}{2}\dfrac{a}{m_c} C^{n-1}\mathbf{s}^{n-1} + \dfrac{\Delta t}{2} dL_{\varphi^{n-1}}\mathbf{s}^{n-1}, \\ 0 = \mathbf{F}^{(c)}(\mathbf{s}^n, \mathbf{c}^n) = \mathbf{c}^n - \mathbf{c}^{n-1} + \frac{\Delta t}{2}\frac{a}{m_s} S^n \mathbf{c}^n + \frac{\Delta t}{2}\frac{a}{m_s} S^{n-1}\mathbf{c}^{n-1}, \end{cases} \tag{4.2}$$

where $\mathbf{s}^n = [s_1^n, s_2^n, \ldots]^\mathsf{T}$, $\mathbf{c}^n = [c_{1/2}^n, c_{3/2}^n, \ldots]^\mathsf{T}$, and

$$\Phi^n = \operatorname{diag}_k^N \left[\frac{\varphi_{k+1/2}^n + \varphi_{k-1/2}^n}{2} \right], \tag{4.3a}$$

$$C^n = \operatorname{diag}_k^N \left[\frac{\varphi_{k+1/2}^n c_{k+1/2}^n + \varphi_{k-1/2}^n c_{k-1/2}^n}{2} \right], \tag{4.3b}$$

$$L_{\varphi^n} = \operatorname{tridiag}_k^N \left[-\varphi_{k-1/2}^n, \varphi_{k-1/2}^n + \varphi_{k+1/2}^n, -\varphi_{k+1/2}^n \right], \tag{4.3c}$$

$$S = \operatorname{diag}_k^N \left[\varphi_{k+1/2}^n \left(\frac{s_{k+1}^n + s_k^n}{2} \right) \right]. \tag{4.3d}$$

Note that equations (4.2) are not linear, since the matrices C, S, L_ϕ, and Φ also depend on $\mathbf{c}^n$ and $\mathbf{s}^n$, either directly or via the (linear) function φ. It is important to note that the matrix L_φ is defined as L_D of (2.4), but it depends only on the half of the unknowns of the problem: precisely, L_φ depends on $\mathbf{c}$ and it multiplies $\mathbf{s}$ in formula (4.2).

The two staggered grids represent a sort of finite difference analogue of the approximation with $P1$ (for $s(x)$) and $P0$ (for $c(x)$) conforming finite elements considered in [2]. The results obtained here on preconditioning should also be applicable with little modifications in that case, too.

Boundary conditions are imposed considering $j = 1, 2, \ldots, N$ in (4.2) and assuming at all timesteps a given value for s_0 (Dirichlet boundary condition at $x = 0$) and that $s_{N+1} = s_{N-1}$ (homogeneous Neumann boundary condition at $x = 1$). Thus the expressions of $\mathbf{F}_1^{(s)}$ and $\mathbf{F}_N^{(s)}$ are modified accordingly with respect to those in (4.2), together with the corresponding elements in the Jacobian (4.4). The $2N$ unknowns are collected in a vector $\mathbf{u}$ with the ordering $\mathbf{u} = [s_1, s_2, \ldots, s_N, c_{1/2}, \ldots, c_{N-1/2}]^\mathsf{T}$.

Both the Crank–Nicholson and the Crandall–Liggett formulas give rise to an unconditionally stable scheme. Following the results previously established, in order to solve the nonlinear problem (4.2), Newton iterations are employed. To this end, one needs the Jacobian matrix, which is naturally split into four $N \times N$ block as

$$J = F' = \left[\begin{array}{c|c} J_s^s & J_c^s \\ \hline J_s^c & J_c^c \end{array} \right], \qquad \mathbf{u} = \begin{pmatrix} \mathbf{u}_s \\ \mathbf{u}_c \end{pmatrix}.$$

The entries (disregarding fixed rank corrections for the boundary conditions) are

(4.4)

$$\begin{aligned}
[J_s^s]_{j,k} =& \frac{\partial \mathbf{F}_j^{(s)}}{\partial s_k} = \frac{\varphi_{j+1/2} + \varphi_{j-1/2}}{2} \delta_{jk} + \frac{\Delta t}{2} \frac{a}{m_c} \frac{\varphi_{j+1/2} c_{j+1/2} + \varphi_{j-1/2} c_{j-1/2}}{2} \delta_{jk} \\
&+ \frac{d}{2} \frac{\Delta t}{h^2} \left[-\varphi_{j-1/2} \delta_{k,j-1} + (\varphi_{j-1/2} + \varphi_{j+1/2}) \delta_{k,j} - \varphi_{j+1/2} \delta_{k,j+1} \right], \\
[J_c^s]_{j,k} =& \frac{\partial \mathbf{F}_j^{(s)}}{\partial c_{k+1/2}} = \frac{\varphi'_{j+1/2} s_j \delta_{jk} + \varphi'_{j-1/2} s_j \delta_{j,k+1}}{2} \\
&+ \frac{\Delta t}{2} \frac{a}{m_c} \frac{(\varphi'_{j+1/2} c_{j+1/2} + \varphi_{j+1/2}) \delta_{jk} + (\varphi'_{j-1/2} c_{j-1/2} + \varphi_{j-1/2}) \delta_{j,k+1}}{2} \\
&+ \frac{d}{2} \frac{\Delta t}{h^2} \left[\varphi'_{j-1/2} (s_j - s_{j-1}) \delta_{j,k+1} - \varphi'_{j+1/2} (s_{j+1} - s_j) \delta_{j,k} \right],
\end{aligned}$$

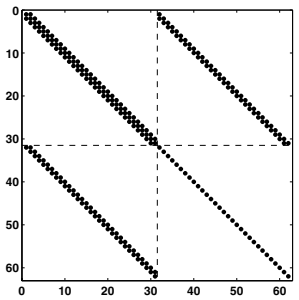

FIG. 5. *Sparsity structure of the Jacobian matrix* (4.4).

$$[J_s^c]_{j,k} = \frac{\partial \mathbf{F}^{(c)}_{j+1/2}}{\partial s_k} = \frac{\Delta t}{2}\frac{a}{m_s}\varphi_{j+1/2}c_{j+1/2}\frac{\delta_{j,k-1}+\delta_{jk}}{2},$$
$$[J_c^c]_{j,k} = \frac{\partial \mathbf{F}^{(c)}_{j+1/2}}{\partial c_{k+1/2}} = \left[1 + \frac{\Delta t}{2}\frac{a}{m_s}(\varphi'_{j+1/2}c_{j+1/2} + \varphi_{j+1/2})\frac{s_{j+1}+s_j}{2}\right]\delta_{jk}.$$

The sparsity structure of the Jacobian matrix with entries defined in (4.4) is shown in Figure 5. In order to guarantee the convergence of the Newton method, a timestep restriction of $\Delta t = O(h)$ is imposed throughout this section, as in Theorem 2.1. A more detailed analysis of the matrix will be carried out in the next section.

4.1. Solving the linear system. At each Newton iteration, one has to solve a linear system with matrix J, which is not symmetric, and thus GMRES is a natural choice for the main Krylov solver.

The top left J_s^s block is given by

$$J_s^s = \Phi + \frac{\Delta t}{2}\frac{a}{m_c}C + \frac{1}{2}\frac{\Delta t}{h^2}dL_\varphi,$$

which is very similar to (2.6), except that the identity is replaced by the diagonal matrix Φ with $O(1)$ entries and the tridiagonal Y term of (2.6) is not present, corresponding instead to the third term of the J_c^s block. The extra term of J_s^s, involving the diagonal matrix C, has entries of order Δt. Hence J_s^s is spectrally not too different from F' of (2.6) and thus the unpreconditioned GMRES iterations count should grow as $\sqrt{N}$, which is indeed confirmed in Figure 6, which graphs the average, minimum, and maximum number of GMRES iterations needed in the case $a = 1$ and for different values of the number of grid points N. A least square fit gives $N^{0.5217}$ for the number of iterations.

In order to devise a preconditioning strategy, given the structure of J_s^s, a V-cycle can be employed on this block if the rest of the matrix can be optimally dealt with. To this end, observe that the lower left block J_s^c has nonzero entries only on two diagonals and these decay as $O(\Delta t)$, while the bottom right block J_c^c is the identity matrix plus a diagonal matrix with $O(\Delta t)$ entries.

THEOREM 4.1. *Assuming $\Delta t = O(h)$, the upper triangular part of J, namely,*

$$P = \left[\begin{array}{c|c} J_s^s & J_c^s \\ \hline \mathbf{0} & J_c^c \end{array}\right], \tag{4.5}$$

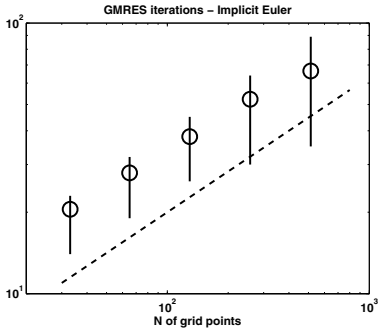

FIG. 6. *Number (average, minimum, and maximum) of unpreconditioned GMRES iterates per timestep with $A = 1$ for 3 values of N. The dashed line indicates the $N^{1/2}$ slope.*

is an optimal preconditioner for J, assuming that the function $\varphi(c)$ is bounded away from 0 (i.e., when the porosity of the gypsum-carbonate mixture is never zero, which corresponds to having $\beta > 0$ in the model of section 3).

Proof. First observe that the diagonal blocks are nonsingular, so that

$$P^{-1} = \left[\begin{array}{c|c} (J_s^s)^{-1} & -(J_s^s)^{-1}(J_c^s)(J_c^c)^{-1} \\ \hline \mathbf{0} & (J_c^c)^{-1} \end{array}\right],$$

and the preconditioned system has matrix

$$P^{-1}J = \left[\begin{array}{c|c} \mathbf{1} - (J_s^s)^{-1}(J_c^s)(J_c^c)^{-1}(J_s^c) & \mathbf{0} \\ \hline (J_c^c)^{-1}(J_s^c) & \mathbf{1} \end{array}\right],$$

where $\mathbf{0}$ denotes the null matrix and $\mathbf{1}$ the identity matrix.

The key point now is that all entries of $P^{-1}J$ are negligible except the diagonal ones. In fact, J_c^c is diagonal with entries equal to $1 + O(\Delta t)$ and thus its inverse has the same property. Since J_s^c is tridiagonal with entries of $O(a\Delta t)$, the same is true for the lower-left block of $P^{-1}J$. Gershgorin circles arising from the lower half of the matrix are thus centered at 1 in the complex plane and have radii decaying as $O(\Delta t)$.

Let us now turn to the upper half of the matrix, where trivially one has that $\| (J_c^s)(J_c^c)^{-1}(J_s^c) \|_\infty = O(\Delta t)$, and thus it suffices to show that $\| (J_s^s)^{-1} \|_\infty$ is bounded to conclude that the Gershgorin circles arising from the upper half of the matrix are centered at $1 + O(\Delta t)$ in the complex plane and have radii decaying as $O(\Delta t)$.

To this end, split

$$J_s^s = Z - W = Z(\mathbf{1} - Z^{-1}W),$$

where Z is the diagonal part, which is

$$Z = \mathrm{diag}_k(z_k), \qquad z_k = \varphi_k + \Delta t \frac{a}{m_c}\widetilde{\varphi}_k + 2\frac{\Delta t}{h^2}\varphi_k,$$

where $\varphi_k = \frac{1}{2}(\varphi_{k+1/2} + \varphi_{k-1/2})$ and $\widetilde{\varphi}_k = \frac{1}{2}(\varphi_{k+1/2}c_{k+1/2} + \varphi_{k-1/2}c_{k-1/2})$. Since Z is diagonal, one easily gets the estimate

$$\|Z^{-1}\|_\infty \le \max_k \frac{1}{z_k} = \frac{h^2}{\Delta t}\max_k \frac{1}{2\varphi_k}\left(1 + O\left(\tfrac{h^2}{\Delta t}\right)\right) = O\left(\tfrac{h^2}{\Delta t}\right).$$

Next observe that $Z^{-1}W = \frac{\Delta t}{h^2}\,\mathrm{tridiag}_k(\frac{1}{z_k}[\varphi_{k-1/2}, 0, \varphi_{k+1/2}])$ and thus

$$\left\|Z^{-1}W\right\|_\infty = \left\|\mathrm{tridiag}_k\left(\frac{[\varphi_{k-1/2}, 0, \varphi_{k+1/2}]}{2\varphi_k + \frac{h^2}{\Delta t}\varphi_k + h^2\frac{a}{m_c}\widetilde{\varphi}_k}\right)\right\|_\infty \leq \max_k \frac{2\varphi_k}{2\varphi_k + \frac{h^2}{\Delta t}\varphi_k + h^2\frac{a}{m_c}\widetilde{\varphi}_k} \leq 1 - Ch$$

for some small positive constant C. Therefore

$$\left\|\left(\mathbf{1} - Z^{-1}W\right)^{-1}\right\|_\infty \leq \sum_{j=0}^{\infty}\left\|Z^{-1}W\right\|_\infty^j \leq \frac{1}{Ch}$$

and

$$\|(J_s^s)^{-1}\|_\infty = \left\|\left(Z\left(\mathbf{1} - Z^{-1}W\right)\right)^{-1}\right\|_\infty \leq \left\|\left(\mathbf{1} - Z^{-1}W\right)^{-1}\right\|_\infty \left\|Z^{-1}\right\|_\infty = O(1). \qquad \square$$

Remark 4.2. When applying the preconditioner, the block triangular system $P\mathbf{y} = \mathbf{b}$ is solved as

$$\mathbf{y}_c = (J_c^c)^{-1}\mathbf{b}_c, \qquad \mathbf{y}_s = (J_s^s)^{-1}(\mathbf{b}_s - J_c^s\mathbf{y}_c),$$

where the deponents s and c refer to the upper and lower halves of the vectors, respectively. The previous result shows that the spectrum of $P^{-1}J$ is strongly clustered at 1 independently on the discretization parameter h, and thus the block preconditioner P is optimal. For the whole preconditioner to be optimal, however, an optimal solver for the J_s^s block is needed. However, J_s^s is the sum of two diagonal matrices and a tridiagonal matrix which is the discretization of a Laplacian operator, regularized with the (strictly positive) function $\varphi(c(x))$, and thus has spectral properties close to those of X_N studied in section 2.3. As in the scalar case, an MGM (e.g., with one damped Jacobi as presmoother and a Galerkin approach with linear interpolation) is an optimal solver for this block.

5. Simulations and performance of the algorithm. Figure 7 shows some typical curves obtained from the simulations with model (3.1). Note that for bigger values a, the reaction is faster and a boundary layer appears. For $a = 10^4$, Figure 8 shows the temporal evolution of the two main variables: while SO_2 penetrates deeper and deeper into the stone (b), calcium carbonate is substituted by the more porous gypsum in a narrow spatial band where the curve $c(t, x)$ presents a boundary layer. Once formed, this transition region travels toward the interior of the stone (a). The self-similarity of the solutions of (3.1) under rescaling of the temporal and spatial variables mentioned at the beginning of section 3 implies that the boundary layer observed for $a = 10^4$ will also appear for lower values of a if the solutions were sought for a larger temporal and spatial domain.

Newton iterations. Figure 9 graphs the average, minimum, and maximum number of Newton iterations used by the numerical method to solve the nonlinear equation (4.2) at each timestep.

For $a = 1$ (black circles), the number of iterations is almost constant when the number of grid points is increased. Furthermore, for a given number of points employed in the discretization, the number of Newton iterations increases very moderately even when a is increased by several orders of magnitude: e.g., for $N = 128$

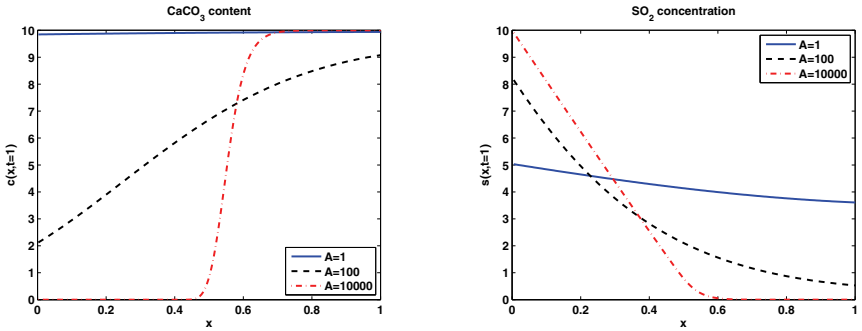

(a) (b)

FIG. 7. *For different values of a, marble content, and SO_2 concentration inside the stone predicted by the model* (3.1) *for* $t = 1$.

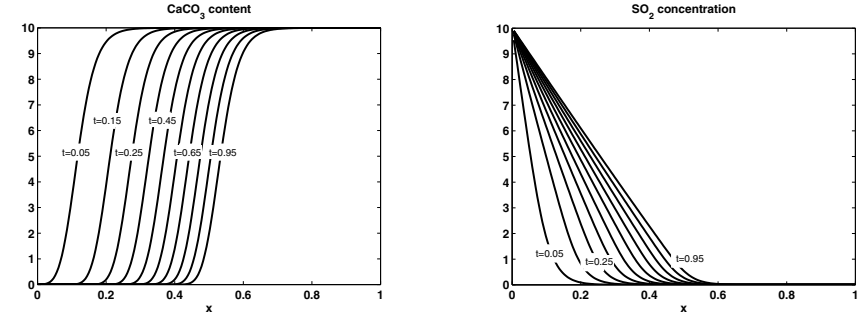

(a) (b)

FIG. 8. *Temporal evolution of the calcium carbonate and sulfate concentration predicted by the model* (3.1) *with* $a = 10^4$.

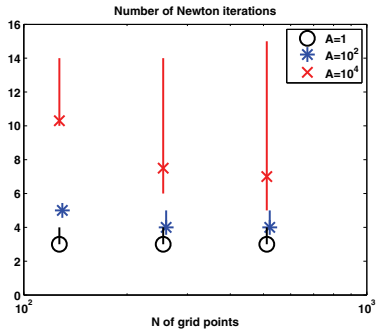

FIG. 9. *Number (average, minimum, and maximum) of Newton iterates per timestep.*

the scheme needs an average of three Newton iterations per timestep for $a = 1$, five for $a = 100$ (blue stars), and ten for $a = 10000$ (red crosses). Finally, note that for higher values of N, the number of Newton iterations decreases slightly since the grid becomes able to resolve the boundary layer better.

Preconditioning. Consider now the Gauss–Seidel preconditioner at block level, with MGM on the (s, s) block. The (c, c) block does not need an inner preconditioner

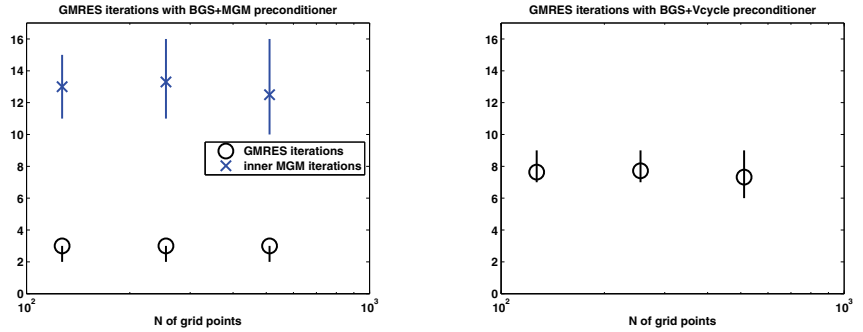

FIG. 10. *Number (average, minimum, and maximum) of GMRES iterates per timestep with* $a = 1$ *for three values of* N. (a) *Block Gauss–Seidel and MGM for the upper left block was used as a preconditioner. Blue crosses and lines refer to the number of inner MGM iterations.* (b) *GMRES iterations when performing only one V-cycle of the MGM.*

since it is diagonal and can be solved directly. This strategy yields an optimal preconditioner, i.e., renders the number of GMRES iterations independent from N, as confirmed by the numerical experiments shown in Figure 10. In panel (a) the MGM driven to convergence is used as solver for the (s, s) block in the preconditioner: GMRES converges in 2–3 iterations, requiring 10–15 MGM cycles at each iteration. In panel (b) only a single MGM V-cycle is employed as inner preconditioner for the (s, s) block: the number of GMRES iterations grows slightly (6–8), but this procedure is overall more efficient. An impressive series of good features can be observed: minimal average computational cost, minimal number of iterations, and minimal variance in the latter number meaning a strong robustness of the procedure.

5.1. Asymptotics for the front position. The asymptotic analysis of [15] predicts that the front of the travelling wave of $c(t, x)$ that separates the gypsum dominated phase from the carbonate dominated phase and that moves inward in the marble sample asymptotically behaves as $x_{\text{front}} \sim \sqrt{t}$.

Numerical experiments were performed to test this prediction and to check how fast the front approaches this asymptotics. In order to perform the comparison, the information on the front position was extracted from the numerical solutions $c^n_{j+1/2}$ by identifying the gypsum-carbonate front with the point with the steepest gradient of $c(t^n, x)$.

For $a = 10^4$, Figure 11(a) shows the position of the front. Note that the step-like behavior of the numerical front that is apparent in some regions of the graph is due to the finite spatial resolution of the simulation ($h = 1/128$). In order to check the asymptotics, the position is also plotted in double logarithmic scale in Figure 11(b), together with the $\sqrt{t}$ slope (dashed line). Note that both simulations agree with the slope of the asymptotics and that for the smaller value of a, the solution approaches the asymptotics more slowly.

6. Sample application in two dimensions. This section presents a numerical simulation of (3.1) in the two-dimensional setting of Figure 4. Consider the domain $\Omega = [0, 1] \times [0, 1]$. When using N points per direction, denote $x_\xi = \xi/N$ and $y_\xi = \xi/N$. The construction of section 4 is generalized considering two staggered grids: the *integer grid* is the set of points $\{(x_i, y_j)\}_{i,j=0}^{N}$ carrying the values $s_{i,j}$ of the SO_2

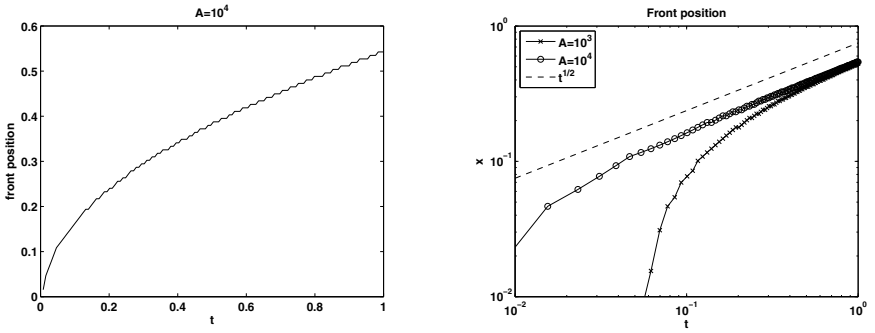

(a) (b)

FIG. 11. *Gypsum-carbonate front position in a sulfation problem: Numerical simulations (solid lines) and predicted asymptotics (dashed line) in* (b).

concentration field $s(x, y)$ and the *half-integer grid* is the set $\{(x_{i+1/2}, y_{j+1/2})\}_{i,j=1}^{N}$ carrying the values $c_{i+1/2,j+1/2}$ of the calcium carbonate concentration field. The discretization of the elliptic operator is then generalized in the usual way to the two-dimensional setting, and the new form of the fixed point problem (4.2) and its Laplacian (4.4) are derived. The numerical scheme now requires, at each timestep, the solution of a system of $2N^2$ nonlinear equations. Again using the Newton method, at each iteration one needs to solve a sparse linear system with a matrix of dimension $2N^2 \times 2N^2$.

The Jacobian matrix has the same block structure described in the one-dimensional case (see also Figure 5). Since it is not symmetric, GMRES is used as the main Krylov solver with specialized structured preconditioners as in the one-dimensional case. The main difference in fact is that now the J_s^s block is a weighted two-dimensional Laplacian plus diagonal corrections that are small (in the sense of order of h). The J_c^c block remains diagonal with elements equal to $1 + O(\Delta t)$, and the preconditioner (4.5) can be applied. The off-diagonal blocks have more nonzero diagonals, but their elements are still small and Theorem 4.1 can be generalized to the two-dimensional setting.

Here, only the best preconditioner among those evaluated in the one-dimensional setting is employed, namely, the upper triangular part of the Jacobian matrix, where only one V-cycle on the (s, s) block is performed. Figure 12 shows the effectiveness of this preconditioning technique. On a 64×64 grid, unpreconditioned GMRES requires an average of 15–20 iterations to solve the Jacobian linear system in each Newton step, with frequent peaks of 24 iterations (blue crosses in the figure are the average values, blue lines the minimum to maximum range). Moreover, the number of iterations is not constant but depends on the timestep. On the contrary, the preconditioned method always employs an average of twelve PGMRES iterations, with little variability both within the timestep and across the different times (black circles and lines).

Figure 13 depicts the solution obtained for $a = 10^3$. Recall that the marble is in contact with the polluted air at the bottom and left boundary (darker regions), while at the top and right boundary free-flow conditions are considered. Both the color code and the isolines refer to the carbonate concentration in the stone. An obvious deformation of the $CaCO_3$ field can be observed near the corner, clearly indicating that SO_2, penetrating from both sides, causes an enhanced loss of material: if the gypsum crust were to fall off here, the sharp edge would be chipped off and the shape of the stone would be permanently changed. This simulation, although performed

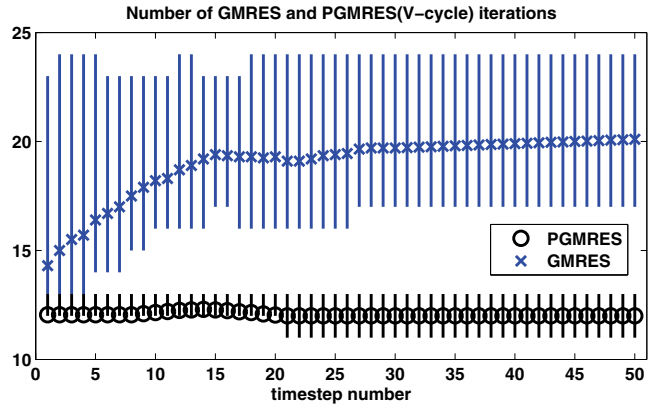

FIG. 12. *Number of GMRES iterations per Newton step: For each timestep the average, minimum, and maximum number of linear iterations are shown. Without preconditioner: blue crosses. With V-cycle preconditioner: black circles.*

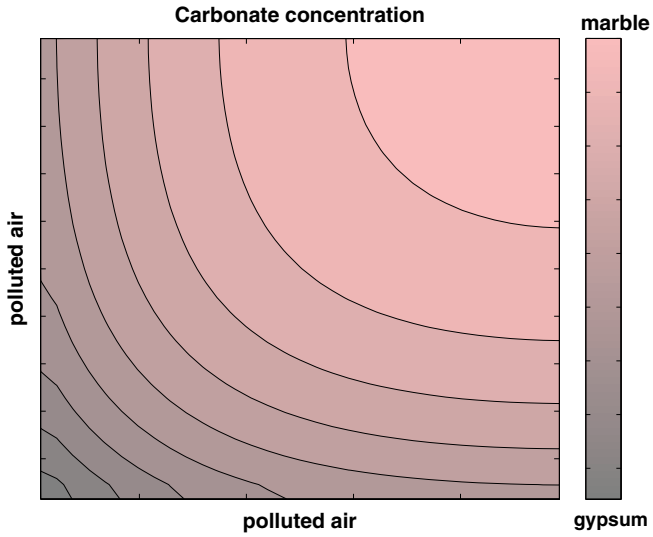

FIG. 13. *Simulation of marble sulfation in two dimensions.*

at low resolution (64×64 grids) and with a moderate value of a, already indicates the relevance of our project of developing accurate numerical simulators for realistic geometries of the domain Ω in two and three dimensions.

7. Conclusions and future developments. The novel contributions of this paper are the proposal of a fully implicit numerical method for dealing with nonlinear PDEs of porous media type and its convergence analysis, and the study of optimal preconditioning strategies for the inner linear systems. In fact, the nonlinear nature of the underlying mathematical model requires the application (at each timestep) of an iterative solver for a large nonlinear system. The classical Newton method can be employed but, at every step, it requires the solution of a large, locally structured, linear system that has been handled using specialized iterative or multi-iterative solvers. In

particular, the spectral analysis of the relevant matrices has been crucial for identifying appropriate preconditioned Krylov methods with efficient V-cycle preconditioners. Numerical experiments for the validation of our analysis complement this contribution, which is aimed at providing a noninvasive tool for a quantitative forecast of the damage evolution in a given monument.

In particular, the application of the above-mentioned techniques to the numerical approximation of a mathematical model describing the damage of marble monuments by the sulfation process was considered. The use of our resulting fast integration algorithms allows us to exploit the model and its predictive power for the strategy known as *planned conservation*, that is, the novel approach that privileges the study and prevention of the damages to delay and optimize the actual restoration works. Both one- and two-dimensional numerical simulations were carried out using simple domains.

For future work, two main directions appear naturally. The first extension is to employ finite element methods for the space discretization in order to deal with more realistic domains in two and three dimensions that can model a real architectural item with a complicated geometry. The other natural extension of the numerical treatment for the sulfation problem involves considering the 3-equations model in [1] and/or a model for a remediation technique, such as the one in [7], which also includes degenerate terms. As a long term goal, being able to simulate both the damage and the remediation process with validated mathematical models and numerical methods would allow us to perform numerical experiments of restoration works.

REFERENCES

[1] G. Alì, V. Furuholt, R. Natalini, and I. Torcicollo, *A mathematical model of sulphite chemical aggression of limestones with high permeability.* I. *Modeling and qualitative analysis*, Transp. Porous Media, 69 (2007), pp. 109–122.

[2] D. Aregba-Driollet, F. Diele, and R. Natalini, *A mathematical model for the sulphur dioxide aggression to calcium carbonate stones: Numerical approximation and asymptotic analysis*, SIAM J. Appl. Math., 64 (2004), pp. 1636–1667.

[3] A. E. Berger, H. Brezis, and J. C. W. Rogers, *A numerical method for solving the problem* $u_t - \Delta f(u) = 0$, RAIRO Numer. Anal., 13 (1979), pp. 297–312.

[4] H. Brézis and A. Pazy, *Convergence and approximation of semigroups of nonlinear operators in Banach spaces*, J. Funct. Anal., 9 (1972), pp. 63–74.

[5] R. Bugini, M. Laurenzi Tabasso, and M. Realini, *Rate of formation of black crusts on marble. A case study*, J. Cultural Heritage, (2000), pp. 111–116.

[6] F. Cavalli, G. Naldi, G. Puppo, and M. Semplice, *High-order relaxation schemes for nonlinear degenerate diffusion problems*, SIAM J. Numer. Anal., 45 (2007), pp. 2098–2119.

[7] F. Clarelli, C. Giavarini, R. Natalini, C. Nitsch, and M. L. Santarelli, *Mathematical models for the consolidation processes in stones*, in Proceedings of the Eu-ARTECH International Symposium: Stone Consolidation in Cultural Heritage—Research and Practice, Lisbon, 2008, to appear.

[8] M. G. Crandall and T. M. Liggett, *Generation of semi-groups of nonlinear transformations on general Banach spaces*, Amer. J. Math., 93 (1971), pp. 265–298.

[9] M. Donatelli, M. Semplice, and S. Serra-Capizzano, *Analysis of multigrid preconditioning for implicit PDE solvers for degenerate parabolic equations*, SIAM J. Matrix Anal. Appl., submitted.

[10] S. Evje and K. H. Karlsen, *Monotone difference approximations of BV solutions to degenerate convection-diffusion equations*, SIAM J. Numer. Anal., 37 (2000), pp. 1838–1860.

[11] K. L. Gauri, N. P. Kulshreshtha, A. R. Punuru, and A. N. Chowdhury, *Rate of decay of marble in laboratory and outdoor exposure*, J. Mater. Civil Eng., 1 (1989), pp. 73–85.

[12] C. Giavarini, M. L. Santarelli, R. Natalini, and F. Freddi, *A nonlinear model of sulphation of porous stones: Numerical simulations and preliminary laboratory assessments*, J. Cultural Heritage, 9 (2008), pp. 14–22.

[13] A. Greenbaum, *Iterative Methods for Solving Linear Systems*, Frontiers Appl. Math. 17, SIAM, Philadelphia, 1997.
[14] F. R. Guarguaglini and R. Natalini, *Global existence of solutions to a nonlinear model of sulphation phenomena in calcium carbonate stones*, Nonlinear Anal. Real World Appl., 6 (2005), pp. 477–494.
[15] F. R. Guarguaglini and R. Natalini, *Fast reaction limit and large time behavior of solutions to a nonlinear model of sulphation phenomena*, Comm. Partial Differential Equations, 32 (2007), pp. 163–189.
[16] W. Hackbusch, *Multigrid Methods and Applications*, Springer Ser. Comput. Math. 4, Springer-Verlag, Berlin, 1985.
[17] F. H. Haynie, *Deterioration of marble*, Durability Build. Mater., 1 (1983), pp. 241–254.
[18] W. T. Lipfert, *Atmospheric damage to calcareous stones: Comparison and reconciliation of recent experimental findings*, Atmos. Environ., 23 (1989), pp. 415–429.
[19] E. Magenes, R. H. Nochetto, and C. Verdi, *Energy error estimates for a linear scheme to approximate nonlinear parabolic problems*, RAIRO Modél. Math. Anal. Numér., 21 (1987), pp. 655–678.
[20] J. M. Ortega and W. C. Rheinboldt, *Iterative Solution of Nonlinear Equations in Several Variables*, Academic Press, New York, 1970.
[21] Y. Saad, *Iterative Methods for Sparse Linear Systems*, 2nd ed., SIAM, Philadelphia, 2003.
[22] S. Serra-Capizzano, *Multi-iterative methods*, Comput. Math. Appl., 26 (1993), pp. 65–87.
[23] S. Serra-Capizzano, *The GLT class as a generalized Fourier analysis and applications*, Linear Algebra Appl., 419 (2006), pp. 180–233.
[24] P. Tilli, *Locally Toeplitz sequences: Spectral properties and applications*, Linear Algebra Appl., 278 (1998), pp. 91–120.
[25] U. Trottenberg, C. W. Oosterlee, and A. Schüller, *Multigrid*, Academic Press, San Diego, 2001.
[26] J. L. Vázquez, *The Porous Medium Equation. Mathematical Theory*, Oxford Math. Monogr., The Clarendon Press, Oxford University Press, Oxford, UK, 2007.